

---

# MetaGS: A Meta-Learned Gaussian-Phong Model for Out-of-Distribution 3D Scene Relighting

---

Yumeng He   Yunbo Wang\*   Xiaokang Yang  
MoE Key Lab of Artificial Intelligence, AI Institute,  
Shanghai Jiao Tong University  
{ymhe, yunbow, xkyang}@sjtu.edu.cn

## Abstract

Out-of-distribution (OOD) 3D relighting requires novel view synthesis under unseen lighting conditions that differ significantly from the observed images. Existing relighting methods, which assume consistent light source distributions between training and testing, often degrade in OOD scenarios. We introduce **MetaGS** to tackle this challenge from two perspectives. First, we propose a meta-learning approach to train 3D Gaussian splatting, which explicitly promotes learning generalizable Gaussian geometries and appearance attributes across diverse lighting conditions, even with biased training data. Second, we embed fundamental physical priors from the *Blinn-Phong* reflection model into Gaussian splatting, which enhances the decoupling of shading components and leads to more accurate 3D scene reconstruction. Results on both synthetic and real-world datasets demonstrate the effectiveness of MetaGS in challenging OOD relighting tasks, supporting efficient point-light relighting and generalizing well to unseen environment lighting maps.

## 1 Introduction

3D scene relighting generates novel lighting effects that interact with the observed 3D environment, with recent advances in learning-based volume rendering offering effective solutions [20, 35, 22, 39, 23, 21, 3, 29]. A typical approach captures a substantial number of multi-view images of a scene under individual lighting conditions, then trains a NeRF or 3D Gaussian splatting (3DGS) model to generalize to new point light positions [27, 12, 8, 40, 7]. Notably, such idealized data requirements are often impractical in real-world scenarios. To simulate a more realistic capturing process, we build on prior work using a **One Light At a Time (OLAT)** setup [33, 13, 1], where training data is collected with a moving point light and a moving camera. Recent studies have further explored low-cost OLAT capture using a smartphone flashlight as the moving light source [5].

While most OLAT methods assume a coherent lighting distribution between training and testing, real-world scenarios often involve light sources that are randomly distributed around the scene, which may result in biased training data. This leads to an **out-of-distribution (OOD)** issue where test-time light sources deviate from the training distribution. This OOD relighting presents a more natural and challenging task, serving as a robust test for evaluating a model’s performance under “*truly*” novel lighting conditions. Compared with the standard OLAT setup, it complicates the learning of true object illumination properties and geometries due to a limited training corpus with entangled, time-varying lighting and viewing directions and, more critically, spatially biased lighting. As shown in Figure 1, existing OLAT methods struggle with the OOD relighting task, often producing unrealistic lighting effects, such as chaotic specular highlights and shadows, due to overfitting to the training samples. Also, because of the lack of generalizability, when new lighting distributions are introduced, they typically require full retraining or finetuning to adapt.

---

\*Corresponding author.

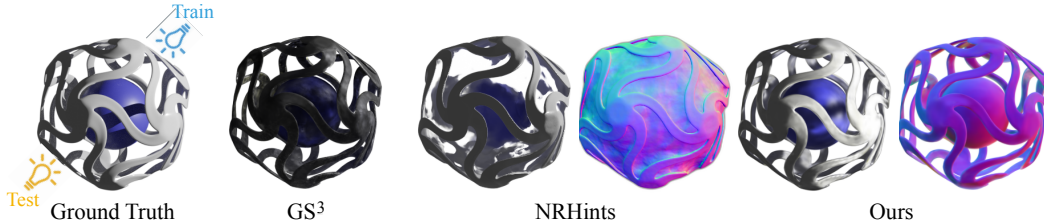


Figure 1: *Preliminary results*: NRHints [33] and GS<sup>3</sup> [1] struggle with out-of-distribution light positions (as specified in Section. 2), as the blurry novel view synthesis results and erroneous normal predictions indicate. GS<sup>3</sup> [1] does not require well-defined surface normals and does not directly output the normal image.

In this paper, we present two novel techniques to enable better OOD relighting. First, we provide a pilot study on **meta-learning-based 3DGS** and introduce MetaGS to mitigate overfitting and improve the generalizability of the OLAT models. This approach leverages bilevel optimization techniques to effectively address the challenges associated with limited training data and complex lighting variations. Specifically, we frame OLAT as a multi-task learning problem, treating rendering under specific lighting positions as distinct tasks. The core idea is to validate the learned Gaussian illumination properties under a given lighting condition using data from other lighting conditions. The resulting second-order gradients of 3DGS parameters can explicitly encourage the model to generalize to unseen illumination rather than overfitting to specific training samples, as is common with standard 3DGS loss functions.

Furthermore, MetaGS integrates simple yet fundamental physical priors into Gaussian splatting by incorporating a **learnable Blinn-Phong reflection model** [2]. This approach effectively decouples different shading components—diffuse, specular, and ambient—leading to a more physically grounded understanding of the interactions between objects and lighting in the training data. This design draws inspiration from prior research [38, 27, 12] indicating that modular and compositional representations enhance generalization capabilities. The decoupled rendering improves the model’s ability to generalize to novel lighting conditions, allowing it to independently adjust each shading component according to the specific lighting scenario.

We evaluate MetaGS on both synthetic and real-world datasets. It supports efficient point-light relighting under highly constrained training illuminations and significantly outperforms existing OLAT methods in OOD relighting tasks. We further demonstrate that both meta-learning and the differentiable Phong model individually contribute to improved generalization. Notably, MetaGS generalizes well to unseen environment maps, despite being trained exclusively in OLAT scenarios.

## 2 Preliminaries

**Definition and challenges of OLAT.** OLAT refers to a specialized setting for 3D reconstruction and relighting. This involves illuminating the subject with a single point light in sequential exposures, capturing one image at each light position. Each capture is represented as a tuple  $\{O_t, V_t, P_t\}$ , where  $O_t$  denotes the observed image,  $V_t$  represents the camera configuration, and  $P_t$  contains lighting information. In our context,  $P_t$  specifies the position of the point light. Unlike the “*multiple lights, multiple cameras*” setup, which requires multi-view images captured by multiple time-synchronized cameras for each lighting condition, OLAT relies on a single camera. This significantly simplifies data collection, particularly in scenarios with dynamic lighting. The rapidly changing light positions in OLAT introduce a new challenge for 3D reconstruction. The color of a 3D point can vary significantly, increasing ambiguity for estimating true object geometries and illumination properties.

**Preliminary findings.** We summarize existing OLAT relighting methods in Table 1. In the preliminary experiments, we evaluate NRHints [33], the prior art in NeRF-based relighting models. We observe that it underperforms in testing scenarios with out-of-distribution (OOD) lighting positions, a feature that we believe should be crucial for relighting methods. Specifically, in Figure 1, the lighting in the training set is arranged on one side of the hemisphere, while the lighting in the test set is arranged on the opposite side (cameras are located on both sides). In such cases, NRHints fails to generate reasonable rendering results, likely due to its implicit modeling of shadows and

Table 1: Comparison of the OLAT relighting methods.

	[34]	[5]	[6]	[33]	[1]	[11]	Ours
Point light	✓	✓	✓	✓	✓	✓	✓
Shadow computation	×	×	✓	✓	✓	✓	✓
OOD light	×	×	×	×	×	×	✓

specular reflections. We additionally evaluate a concurrent 3DGS-based approach [1] and observe similar degraded results under the OOD relighting setup. These findings highlight that understanding intrinsic illumination properties under arbitrary lighting variations remains a challenging task, as the model tends to overfit to perspective-constrained observations and fail to leverage enough physical principles when dealing with unseen lighting distribution.

### 3 Method

In this section, we present the details of MetaGS for addressing the OOD OLAT learning challenge:

- Sec. 3.1: We incorporate physical shading priors within Gaussian splatting via a differentiable Phong reflection model to decouple mixed illumination components.
- Sec. 3.2: We introduce a bilevel optimization scheme to estimate light-independent scene geometries and intrinsic illumination properties, marking an early effort in volume rendering.
- Sec. 3.3: We discuss the entire training pipeline and the implementation details.

#### 3.1 Differentiable Phong Model

Our *MetaGS* method leverages simple yet generalizable physical priors from the Blinn-Phong model [18], which captures three fundamental components of light transport: ambient, diffuse, and specular reflections. The core idea is to disentangle these illumination components by learning the interactions between (i) the normal vectors of the Gaussian points, (ii) the viewing directions, and (iii) the ray direction from the point light.

Specifically, the ambient component represents constant environmental illumination, simulating indirect scattering from surrounding surfaces to establish a baseline brightness level. The diffuse component, based on Lambertian law, describes light scattering in multiple directions from rough surfaces. The specular reflection is computed based on the angle between the light direction and the bisector ( $\mathbf{h}$ ) between the viewing direction ( $\mathbf{v}$ ) and the light direction ( $\mathbf{l}$ ), with a shininess exponent that represents different degrees of glossiness.

In MetaGS, we extend the original 3DGS by introducing the decoupled computation for different shading components. As shown in Figure 2, in addition to the basic Gaussian attributes (*e.g.*, position  $\mathbf{x}$ , rotation  $R$ , scale  $S$ , opacity  $\alpha$ , and spherical harmonic coefficients  $f$ ), each Gaussian point is further associated with a normal vector  $\mathbf{n}$ , a 3-channel diffuse color  $k_d$ , and a 1-channel specular coefficient  $k_s$ . The newly added attributes enhance the model’s understanding of lighting effects, facilitating the learning process of light-independent object geometries. The overall color of a Gaussian point is determined by:

$$L_p = L_a + L_d + L_s = L_a + \sum_{|\text{lights}|} (k_d I_d + k_s I_s), \quad (1)$$

where  $k_{\{d,s\}}$  and  $I_{\{d,s\}}$  are the colors and intensities of the diffuse and specular components.  $|\text{lights}|=1$  in OLAT. In graphics, zero-order spherical harmonics (SH) coefficients typically represent the basic, uniform component of a function defined over the sphere, essentially the average or constant part of a lighting environment. Therefore, we restrict Gaussians’ SH coefficients to zero order, denoted by  $f_0$ , corresponding to the ambient color. We compute the diffuse and specular light transports by multiplying the color and intensity of each component, where the intensities  $I_d$  and  $I_s$  are defined as:

$$I_d = \frac{I}{r^2} \max(0, \mathbf{n} \cdot \mathbf{l}), \quad I_s = \frac{I}{r^2} \max(0, \mathbf{n} \cdot \mathbf{h})^p, \quad (2)$$

where  $I$  denotes the light emitted intensity, which is a global learnable parameter,  $\mathbf{l}$  denotes the point-to-light normalized vector, and  $\mathbf{h} = \frac{\mathbf{v} + \mathbf{l}}{\|\mathbf{v} + \mathbf{l}\|}$  denotes the bisector of the point-to-camera normalized

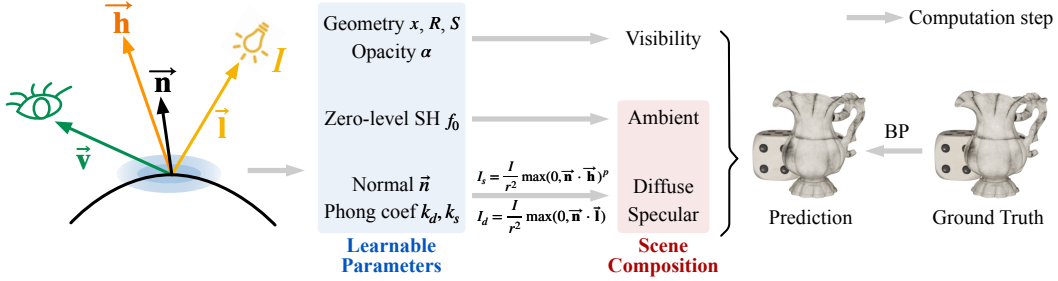


Figure 2: *The model design of MetaGS*: Our model decomposes the illumination effects by interacting the learned Gaussian points with rays originating from both the viewer and the light source.

vector  $\mathbf{v}$  and  $\mathbf{l}$ . We model the coefficients  $k_d$  and  $k_s$  implicitly, where  $k_s$  is multiplied by the RGB color of the point light.

**Shadow computation.** We calculate shadow effects using a BVH-based ray tracing method [7]. Similar to the camera-to-point accumulated transmittance, the received light intensity  $T_i^{\text{light}}$  represents the total transmittance of light along the light-to-point ray. It is therefore affected by the opacity of the surfaces encountered along this path. For each point, we determine light visibility by tracing a ray from the Gaussian’s center to the light source. Since only the diffuse and specular colors are influenced by incident light intensity, we update the color of each point by incorporating the light visibility factor into the diffuse and specular terms from Eq. (1):

$$L_p = L_a + T_i^{\text{light}} \sum_{|\text{lights}|} (k_d I_d + k_s I_s). \quad (3)$$

This explicit formulation accounts for physics-based shadowing effects, provides strong interpretability, and improves generalizability compared to the implicit, high-dimensional shadow modeling methods. However, integrating this module directly into MetaGS’s pipeline presents challenges. Under OLAT conditions, learning coherent geometry is challenging, leading to difficulties in accurately separating shadows from the scene. This, in turn, results in erroneous color predictions. The following meta-learning scheme promotes the mutual learning of scene geometry and appearance, alleviating the difficulties in learning coherent attributes under varying illuminations.

### 3.2 Meta-Learned Gaussian Relighting

Existing 3D relighting methods exhibit performance degradation when handling out-of-distribution relighting, primarily due to overfitting lighting patterns to perspective-constrained observations, resulting in producing unreasonable lighting components (such as wrong specular and shadows).

To address this, we introduce a meta-learning framework based on bilevel optimization, which has been shown to effectively bridge the distribution shift between the training and testing domains, facilitating the generalization of optimized variables to unseen scenarios [4]. This training strategy can also promote coherent geometry learning in complex OLAT tasks, as shown in the ablation study. In MetaGS, the intuition of incorporating bilevel gradient update is to mitigate overfitting to specific light conditions by explicitly simulating test samples with OOD light sources during each gradient update, thereby improving the model’s ability to generalize to varied lighting scenarios.

As illustrated in Alg. 1, we organize the training processes with different  $\{O_t, V_t, P_t\}$  as multiple learning tasks. We alternate model training between these tasks, validating the optimized variables under one lighting condition using data sampled from other conditions. This learning procedure encourages both the lighting attributes ( $f, k_a, k_s$ ) and the geometric attributes ( $\mathbf{x}, \mathbf{n}, R, S, \alpha$ ) of the Gaussian points to converge cohesively.

To simulate test-time conditions, the training data is divided into support (*training*) and query (*validation*) sets. At each iteration,  $2m$  samples are drawn from the training data to form the support set  $\mathcal{D}_{1:m}^{\text{sup}}$  and query set  $\mathcal{D}_{1:m}^{\text{query}}$  (Line 5). Each support sample pairs with a query sample, denoted by subscript  $i$ . During each training step, the model alternates between these tasks in the inner optimization loop (Lines 6-9) and the outer loop (Line 10).

---

**Algorithm 1** Meta-Training for OOD Relighting

---

```
1: Input: Training set  $\{\mathcal{D}_t\}_{1:T}$ , where  $D_t = \{\text{light position, camera parameters, RGB image}\}$ 
2: Hyperparameters: Learning rates  $\alpha, \beta$ 
3: Initialized parameters: Pretrained Gaussian attributes  $\{\theta_k\}$ , where  $\theta_k = (\mathbf{x}, \mathbf{n}, R, S, \alpha, f_0, k_d, k_s)$ 
4: while not converge do
5:   Sample disjoint data  $\mathcal{D}_{1:m}^{\text{sup}}$  and  $\mathcal{D}_{1:m}^{\text{query}}$  from  $\{\mathcal{D}_t\}_{1:T}$ 
6:   for task  $i$  in  $\{1 : m\}$  do ▷ Inner optimization loop
7:      $\theta'_i \leftarrow \theta - \alpha \nabla_{\theta} \mathcal{L}_{\text{final}}(\theta; \mathcal{D}_i^{\text{sup}})$ 
8:   end for
9:    $\{\theta\} \leftarrow \{\theta\} - \beta \sum_{i=1}^m \nabla_{\theta} \mathcal{L}_{\text{final}}(\theta'_i; \mathcal{D}_i^{\text{query}})$  ▷ Outer optimization step
10: end while
```

---

**Inner optimization loop.** In the inner loop, the model is trained on each support set to independently generate  $m$  sub-models, representing the hypothetical estimates  $\theta'_i$  under each lighting condition. All sub-models start with the same parameters of  $\theta$ . The light intensity  $I$  is a global parameter that is also learnable and optimized jointly with the Gaussian attributes. It is omitted here for clarity. We specify the loss function  $\mathcal{L}_{\text{final}}$  in subsequent Sec. 3.3.

**Outer optimization loop.** In the outer loop, a global gradient update is performed across all sampled tasks, updating the Gaussian attributes. We first compute the loss function for each query sample,  $\mathcal{L}_{\text{final}}(\cdot, \cdot; \mathcal{D}_i^{\text{sup}})$ , using the corresponding inner-loop model hypotheses  $\theta'_i$ . We then aggregate the  $m$  losses to update the initial  $\theta$ . This approach, involving task-specific adaptation followed by a global update, enables the model to learn generalizable representations across varying lighting conditions.

### 3.3 Entire Training Pipeline

We employ a three-stage training scheme. The first stage, similar to 3DGS, focuses on training the core Gaussian attributes, including position  $\mathbf{x}$ , rotation  $R$ , scale  $S$ , opacity  $\alpha$ , and spherical harmonic coefficients  $f$ . After this stage, the model tends to capture a rough geometry and an average color across different illuminations, serving as an effective initialization for further refinement. In the second stage, we incorporate the normal attributes into the optimization process, acknowledging that learning a Phong model heavily relies on accurate normal estimations. In the final stage, we integrate the diffuse and specular components, training all parameters concurrently through meta-learning.

**Objective functions.** We follow 3DGS [9] to compute the deviation of the predicted image from the ground truth, using an L1 regularization and a D-SSIM term as the RGB loss. We also employ a sparse loss [8] to encourage the opacity values  $\alpha$  of the Gaussian spheres to approach either 0 or 1, thereby facilitating learning with opaque objects. For normal estimation, we follow GaussianShader [8] to compute the normal vectors using Gaussian’s shortest axis direction, and progressively align them with the depth-inferred pseudo-normals.

**Implementation details.** We implement MetaGS using PyTorch [17]. For optimization, we use the Adam optimizer [10] with the same parameters as those specified by [9]. A consistent set of hyperparameters is applied across all scenes, with details provided in the Appendix. Our training procedure contains three stages: the first two stages each last for  $4k$  iterations, followed by the final meta-learning stage of  $5k$  iterations. The entire training process requires roughly one hour on a single NVIDIA RTX 3090 GPU.

## 4 Experiments

### 4.1 Experimental Settings

We perform three types of OLAT relighting experiments:

- *OOD relighting:* We introduce a novel synthesis setup to assess the generalizability of 3D relighting models under OOD lighting conditions. The point lights in the training set are positioned on one side of the upper hemisphere, while the lighting in the test set is placed on the opposite side.
- *Camera-light-colocated relighting:* This setup mirrors the one used in IRON [34], where the camera and point light are co-located for each image. Similar to the OOD setting, the colocated

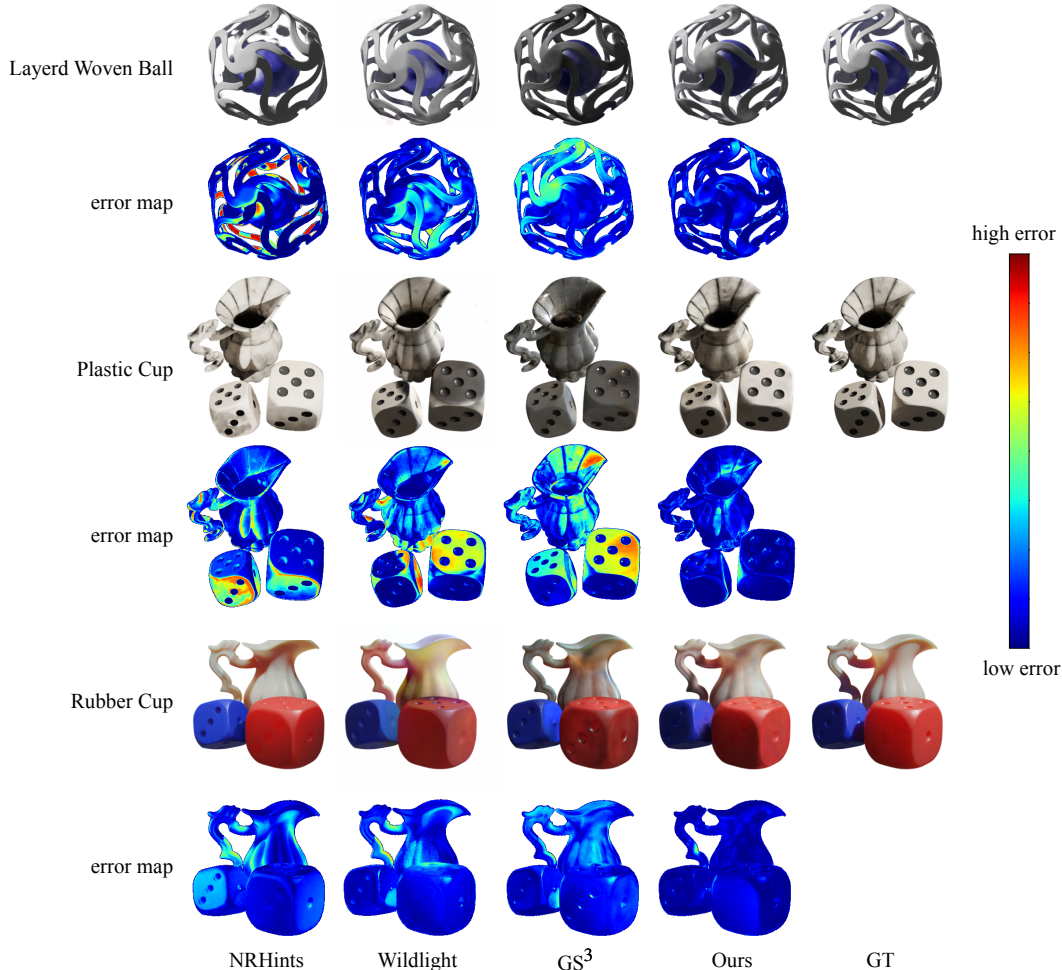


Figure 3: *OOD relighting results on synthetic data*: We present rendered novel views and error maps. While baselines often misrepresent shadows or light-dependent effects (e.g., incorrect shadows in *Plastic Cup*), our model better infers surface appearance.

Table 2: *PSNR results for OOD relighting*. See our Appendix for full comparisons.

Method	Synthetic			Real-world						
	Ball	PlasCup	RubCup	Cat	Catsmall	CupFabric	Fish	FurScene	Pikachu	Pixiu
NRHints [33]	17.25	23.92	27.44	18.04	24.63	24.65	22.57	21.55	24.00	23.03
WildLight [5]	21.73	20.95	24.02	18.65	22.53	24.03	21.47	20.33	19.09	20.22
GS <sup>3</sup> [1]	18.84	20.30	24.37	17.66	23.34	25.04	21.12	17.34	24.11	19.63
Ours	<b>26.76</b>	<b>27.54</b>	<b>27.95</b>	<b>26.45</b>	<b>26.44</b>	<b>27.29</b>	<b>24.68</b>	<b>24.82</b>	<b>25.54</b>	<b>25.65</b>

configuration also represents a constrained lighting regime, as the light source is fixed to the camera pose. For fair comparison, we generate colocated versions of the synthetic scenes accordingly.

- *Environment map relighting*: We evaluate the generalization of the models exclusively trained in the OLAT setup to novel view synthesis with unseen environment lighting maps.

We evaluate MetaGS on 3 synthetic scenes and 7 real captured scenes from NRHints [33], featuring a diverse range of materials, complex object shapes, significant self-occlusion, and intricate shadow effects. Each image is rendered (or captured) with a unique camera pose and point-light position. Full details of the datasets are provided in the Appendix.

For each synthetic scene, we generate a total of 600 OLAT images using Blender, with 500 for training and 100 for testing, following out-of-distribution or colocated data patterns. For the real-world scenes,

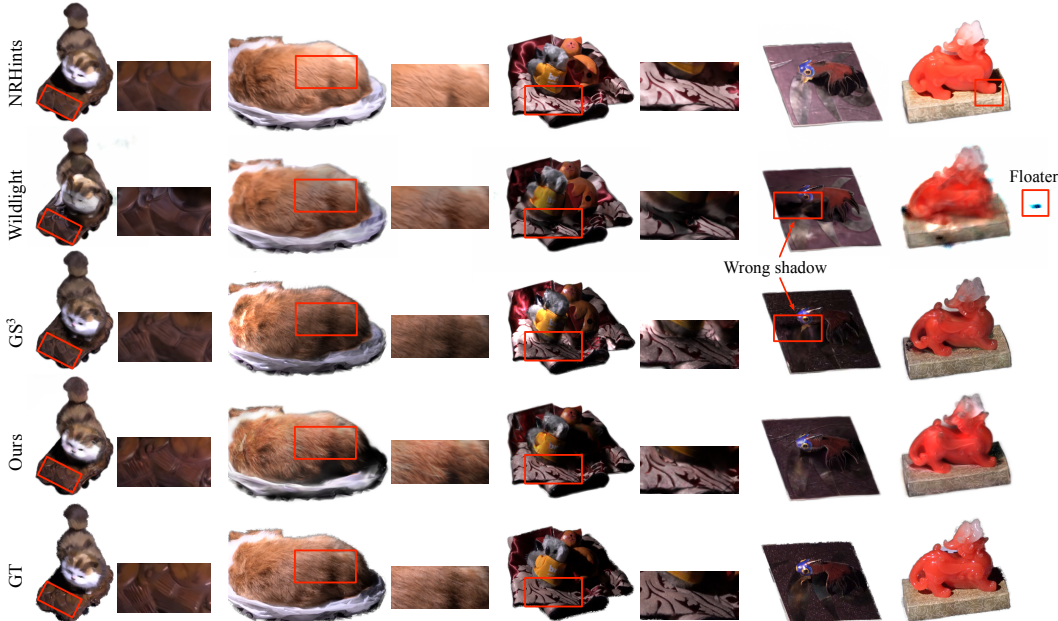


Figure 4: *OOD relighting results on real-world data*: As highlighted with the red boxes, baseline models struggle with some level of global shading consistency, such as color shifts, wrong shadows, and floating artifacts. Our approach presents physically plausible specular highlights and geometrically consistent shadows that closely match ground truths.

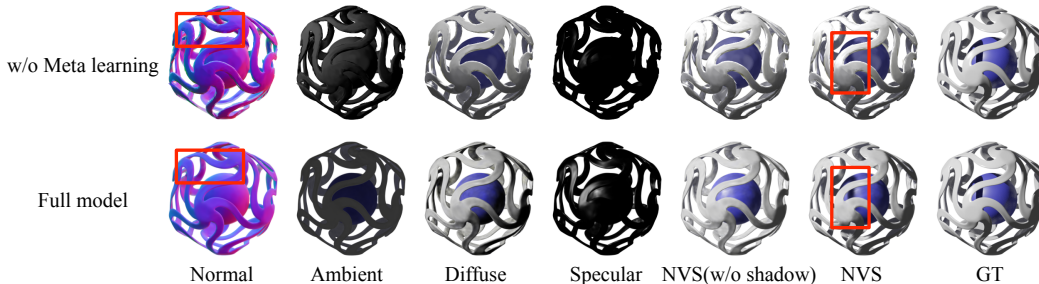


Figure 5: *Ablation studies with qualitative results*: As shown in the decoupling components, the meta-learning scheme is essential for learning object illumination properties and geometries. Without it, the model generates plain lighting effects, particularly for the diffuse and specular components.

we split the data according to their point light positions to construct out-of-distribution datasets, and use 600 training images per scene—a significantly smaller subset than the full NRHints dataset.

We compare MetaGS against both NeRF-based and Gaussian-based models, with a particular focus on the OOD relighting setup. The baseline models include state-of-the-art approaches from the past two years: GS<sup>3</sup> [1], NRHints [33], WildLight [5], Relightable 3DGS [7], GaussianShader [8], and IRON [34]. The evaluation metrics include PSNR, SSIM [24], and LPIPS [37].

## 4.2 Results for Out-of-distribution OLAT Relighting

We evaluate MetaGS in scenarios with OOD point light positions to explore its generalizability to unseen illuminations. The qualitative and quantitative results are respectively presented in Figure 3, Figure 4, and Table 2. Our model remarkably outperforms the baselines in handling complex light interactions. For example, in Figure 4, the lighting and shading effects on the cat’s fur are rendered with high fidelity, while baseline models tend to produce incorrect color tones. Furthermore, as indicated by the error maps in Figure 3, all of three OLAT baselines tend to provide unrealistic results, especially for regions with significant specular reflections or shadows. Please see our Appendix for video visualizations on OOD relighting, where baselines’ performance drops as the light enters the OOD region, while our model provides better relighting results.



Figure 6: *Relighting with environment maps*: Our method, trained under OLAT settings, successfully generalizes to unseen environmental lighting; while the compared method is trained in an all-light-on setup that provides multiple lighting conditions per training view, it still fails to generalize to perform relighting with novel environment maps and exhibits visible artifacts.

The generalizability of MetaGS to OOD illumination stems from two key factors. First, it is due to the Phong model’s ability to capture the underlying principles of light interaction. For example, instead of simply viewing specular highlights as the view-dependent color of a point (which is not generalizable), our method explicitly calculates the interactions of rays and surface normals, enabling the model to generate accurate highlights even in areas not directly illuminated during training. Second, meta-learning further enhances generalization by simulating test-time conditions during training, effectively reducing overfitting to specific illuminations. In the Appendix, we empirically show that the benefit of meta-learning does not come from a larger batch size.

**Ablation studies.** We conduct a series of ablation studies to validate the effectiveness of the meta-learning scheme as well as the shadow computing. From Table 3 and Figure 5, we observe that the proposed meta-learning training scheme strongly impacts performance. Without it, the model struggles to converge smoothly and make unrealistic component estimations, resulting in plain rendering quality.

Table 3: *Ablation studies of each model component for OOD relighting*. We show the average results of all three synthetic scenes.

Method	PSNR <sup>↑</sup>	SSIM <sup>↑</sup>	LPIPS <sup>↓</sup>
Full model	<b>27.42</b>	<b>0.9546</b>	<b>0.0505</b>
w/o Meta-learning	19.14	0.8781	0.0892
w/o Shadow	21.53	0.9105	0.0735

### 4.3 Generalization to Other Relighting Setups with Constrained OLAT Training

**Camera-light-located relighting.** We evaluate MetaGS in the camera-light-located setup, as introduced by IRON [34]. Like the OOD scenario, the colocated setup also imposes limited lighting diversity, as the point light is tied to the camera’s position throughout training. Quantitative results in Table 4 show that MetaGS outperforms IRON, achieving more accurate illumination inference under new point positions, and generating fewer rendering artifacts. Visualizations corresponding to these results can be found in the Appendix.

Table 4: *Novel view synthesis results in PSNR under camera-light-located relighting setup*. Full results in all evaluation metrics are included in the Appendix.

Method	Ball	PlaCup	RubCup
IRON [34]	26.99	34.43	36.22
Ours	<b>38.72</b>	<b>36.90</b>	<b>38.89</b>

**Environment map generalization.** Our model generalizes effectively to environment map relighting. We approximate global illumination by importance sampling point lights from the environment map based on their pixel intensities. Notably, for our model in particular (unlike the compared methods), the sampled light directions at test time may follow a distribution different from those encountered during training, presenting a significant challenge for OOD generalization. Instead of assuming infinite light source distance, we simulate distant lighting by placing point lights along environment directions at a fixed distance (twice the scene radius). We compare our method with R3G [7] and GaussianShader [8]. Both methods fail to converge when trained directly on out-of-distribution (OOD) data, so we construct training data that covers the full hemispherical illumination space.

Even with this setup, GaussianShader still fails to converge, while Relightable 3DGS struggles with the OLAT learning task and exhibits noticeable artifacts. As shown in Figure 6, MetaGS produces diverse and visually plausible relighting results under complex environment maps, demonstrating its robustness and generalization capability.

**More results.** To validate MetaGS’s capability in handling complex lighting conditions, we conduct experiments with test sets containing 2–3 light sources. We also present the results for free-viewpoint relighting with in-distribution point light positions. Please refer to the Appendix for details.

## 5 Related Work

Recent differentiable volume rendering techniques, including NeRF-based [16], SDF-based [31, 32], and 3DGS-based [9] methods, have significantly improved the quality and efficiency of novel view synthesis for 3D scenes. NeRF-based methods utilize deep neural networks to model volumetric scene functions, encoding color and density to synthesize high-quality images from sparse viewpoints [16, 14, 36]. However, these approaches typically require substantial training time. 3DGS significantly reduces both training and inference time. It converts point cloud data into a continuous volumetric representation by applying Gaussian kernels to point cloud data, facilitating rendering and further processing. This technique is now widely adopted for efficient 3D and 4D reconstructions across varied data types [27, 8, 15, 25, 30].

The task of 3D relighting involves altering the illumination in a 3D scene while maintaining its geometry. It requires decomposing materials and lighting of a scene from multiple images, which is challenging due to its high-dimensional nature. Recent advances in volume rendering have introduced various solutions for this task, including those based on neural fields [38, 26, 21, 19, 20, 12, 22, 21, 29] and the methods based on Gaussian point clouds [27, 8, 7, 35]. A limitation of these methods is that they require a substantial volume of multi-view images captured under individual lighting conditions, making them impractical in real-world scenarios. Several studies have proposed NeRF-based 3D relighting techniques within the OLAT framework [28, 38, 33], which greatly reduce the demands on training data. Nonetheless, these techniques tend to be computationally intensive because of NeRF’s inherent complexity in the volume rendering process. In parallel, concurrent 3DGS-based approaches [6, 1] have also explored the OLAT relighting challenge. Despite their efforts, these approaches still face difficulties when dealing with lighting conditions not encountered during training, similar to the limitations observed in NeRF-based methods.

In contrast, our method addresses this issue by incorporating specific physical priors, represented by the Phong reflection model, into the Gaussian splatting framework. We have also designed a meta-learning approach to enhance the method’s generalizability to OOD relighting scenarios.

## 6 Conclusions and Limitations

In this paper, we explored a novel and challenging problem: out-of-distribution (OOD) 3D relighting. To address this, we proposed MetaGS, which builds on Gaussian splatting and presented a novel bilevel optimization-based meta-learning framework that explicitly promotes generalizable Gaussian geometry and appearance learning. This meta-learning formulation allows the model to adapt to varying light sources and viewpoints, even when the training data is biased or sparsely sampled in the lighting space. Furthermore, MetaGS incorporates a differentiable Blinn-Phong reflection model within Gaussian splatting, effectively disentangling lighting effects into ambient, diffuse, and specular shading components, thereby improving the physical realism and reconstruction fidelity under diverse lighting. Extensive experiments on both synthetic and real-world datasets demonstrate that MetaGS significantly outperforms existing OLAT relighting approaches under OOD relighting conditions. It also achieves strong generalization to complex environment maps.

Despite these advances, several limitations remain. An open challenge is ensuring the robustness of our approach under more complex lighting conditions. Moreover, our current framework only accounts for direct illumination; incorporating indirect lighting could further enhance the quality of relighting. Additionally, the current model assumes simple Phong reflection, which may limit fidelity when modeling materials with strong subsurface scattering or anisotropic reflectance.

## References

- [1] Zoubin Bi, Yixin Zeng, Chong Zeng, Fan Pei, Xiang Feng, Kun Zhou, and Hongzhi Wu. GS<sup>3</sup>: Efficient relighting with triple gaussian splatting. In *ACM SIGGRAPH Asia*, 2024.
- [2] James F Blinn. Models of light reflection for computer synthesized pictures. In *ACM SIGGRAPH*, pages 192–198, 1977.
- [3] Yeonjin Chang, Yearim Kim, Seunghyeon Seo, Jung Yi, and Nojun Kwak. Fast sun-aligned outdoor scene relighting based on TensorRF. In *WACV*, pages 3626–3636, January 2024.
- [4] Jiaxin Chen, Xiao-Ming Wu, Yanke Li, Qimai Li, Li-Ming Zhan, and Fu-lai Chung. A closer look at the training strategy for modern meta-learning. *NeurIPS*, 33:396–406, 2020.
- [5] Ziang Cheng, Junxuan Li, and Hongdong Li. WildLight: In-the-wild inverse rendering with a flashlight. In *CVPR*, pages 4305–4314, 2023.
- [6] Jiahui Fan, Fujun Luan, Jian Yang, Miloš Hašan, and Beibei Wang. RNG: Relightable neural Gaussians. *arXiv preprint arXiv:2409.19702*, 2024.
- [7] Jian Gao, Chun Gu, Youtian Lin, Hao Zhu, Xun Cao, Li Zhang, and Yao Yao. Relightable 3D Gaussian: Real-time point cloud relighting with BRDF decomposition and ray tracing. *arXiv preprint arXiv:2311.16043*, 2023.
- [8] Yingwenqi Jiang, Jiadong Tu, Yuan Liu, Xifeng Gao, Xiaoxiao Long, Wenping Wang, and Yuexin Ma. GaussianShader: 3D Gaussian splatting with shading functions for reflective surfaces. In *CVPR*, pages 5322–5332, 2024.
- [9] Bernhard Kerbl, Georgios Kopanas, Thomas Leimkühler, and George Drettakis. 3D Gaussian splatting for real-time radiance field rendering. *TOG*, 42(4):1–14, 2023.
- [10] Diederik P Kingma and Jimmy Ba. Adam: A method for stochastic optimization. *arXiv preprint arXiv:1412.6980*, 2014.
- [11] Zhiyi Kuang, Yanchao Yang, Siyan Dong, Jiayue Ma, Hongbo Fu, and Youyi Zheng. Olat gaussians for generic relightable appearance acquisition. In *SIGGRAPH Asia 2024 Conference Papers*, pages 1–11, 2024.
- [12] Ruofan Liang, Huiting Chen, Chunlin Li, Fan Chen, Selvakumar Panneer, and Nandita Vijaykumar. ENVDR: Implicit differentiable renderer with neural environment lighting. In *ICCV*, pages 79–89, 2023.
- [13] Zhihao Liang, Qi Zhang, Ying Feng, Ying Shan, and Kui Jia. GS-IR: 3D Gaussian splatting for inverse rendering. In *CVPR*, pages 21644–21653, 2024.
- [14] Lingjie Liu, Jiatao Gu, Kyaw Zaw Lin, Tat-Seng Chua, and Christian Theobalt. Neural sparse voxel fields. *NeurIPS*, 33:15651–15663, 2020.
- [15] Jonathon Luiten, Georgios Kopanas, Bastian Leibe, and Deva Ramanan. Dynamic 3D Gaussians: Tracking by persistent dynamic view synthesis. In *3DV*, pages 800–809. IEEE, 2024.
- [16] Ben Mildenhall, Pratul P Srinivasan, Matthew Tancik, Jonathan T Barron, Ravi Ramamoorthi, and Ren Ng. NeRF: Representing scenes as neural radiance fields for view synthesis. *Communications of the ACM*, 65(1):99–106, 2021.
- [17] Adam Paszke, Sam Gross, Francisco Massa, Adam Lerer, James Bradbury, Gregory Chanan, Trevor Killeen, Zeming Lin, Natalia Gimelshein, Luca Antiga, et al. Pytorch: An imperative style, high-performance deep learning library. *NeurIPS*, 32, 2019.
- [18] Bui Tuong Phong. Illumination for computer generated pictures. In *Seminal graphics: pioneering efforts that shaped the field*, pages 95–101. 1998.
- [19] Kripasindhu Sarkar, Marcel C Bühler, Gengyan Li, Daoye Wang, Delio Vicini, Jérémy Riviere, Yinda Zhang, Sergio Orts-Escolano, Paulo Gotardo, Thabo Beeler, et al. LitNeRF: Intrinsic radiance decomposition for high-quality view synthesis and relighting of faces. In *ACM SIGGRAPH Asia*, pages 1–11, 2023.
- [20] Pratul P. Srinivasan, Boyang Deng, Xiuming Zhang, Matthew Tancik, Ben Mildenhall, and Jonathan T. Barron. NeRV: Neural reflectance and visibility fields for relighting and view synthesis. In *CVPR*, pages 7495–7504, June 2021.
- [21] Jia-Mu Sun, Tong Wu, Yong-Liang Yang, Yu-Kun Lai, and Lin Gao. SOL-NeRF: Sunlight modeling for outdoor scene decomposition and relighting. In *ACM SIGGRAPH Asia*, pages 1–11, 2023.
- [22] Marco Toschi, Riccardo De Matteo, Riccardo Spezialetti, Daniele De Gregorio, Luigi Di Stefano, and Samuele Salti. Relight My Nerf: A dataset for novel view synthesis and relighting of real world objects. In *CVPR*, pages 20762–20772, June 2023.
- [23] Dongqing Wang, Tong Zhang, and Sabine Süssstrunk. NEMTO: Neural environment matting for novel view and relighting synthesis of transparent objects. In *ICCV*, pages 317–327, October 2023.

- [24] Zhou Wang, Alan C Bovik, Hamid R Sheikh, and Eero P Simoncelli. Image quality assessment: from error visibility to structural similarity. *IEEE transactions on image processing*, 13(4):600–612, 2004.
- [25] Guanjun Wu, Taoran Yi, Jiemin Fang, Lingxi Xie, Xiaopeng Zhang, Wei Wei, Wenyu Liu, Qi Tian, and Xinggang Wang. 4D Gaussian splatting for real-time dynamic scene rendering. In *CVPR*, pages 20310–20320, 2024.
- [26] Tong Wu, Jia-Mu Sun, Yu-Kun Lai, and Lin Gao. DE-NeRF: Decoupled neural radiance fields for view-consistent appearance editing and high-frequency environmental relighting. In *ACM SIGGRAPH*, pages 1–11, 2023.
- [27] Tong Wu, Jia-Mu Sun, Yu-Kun Lai, Yewen Ma, Leif Kobbelt, and Lin Gao. DeferredGS: Decoupled and editable Gaussian splatting with deferred shading. *arXiv preprint arXiv:2404.09412*, 2024.
- [28] Yingyan Xu, Gaspard Zoss, Prashanth Chandran, Markus Gross, Derek Bradley, and Paulo Gotardo. ReNeRF: Relightable neural radiance fields with nearfield lighting. In *ICCV*, pages 22581–22591, 2023.
- [29] Siqi Yang, Xuanning Cui, Yongjie Zhu, Jiajun Tang, Si Li, Zhaofei Yu, and Boxin Shi. Complementary intrinsics from neural radiance fields and CNNs for outdoor scene relighting. In *CVPR*, pages 16600–16609, June 2023.
- [30] Ziyi Yang, Xinyu Gao, Wen Zhou, Shaohui Jiao, Yuqing Zhang, and Xiaogang Jin. Deformable 3D Gaussians for high-fidelity monocular dynamic scene reconstruction. In *CVPR*, pages 20331–20341, 2024.
- [31] Lior Yariv, Jiatao Gu, Yoni Kasten, and Yaron Lipman. Volume rendering of neural implicit surfaces. *NeurIPS*, 34:4805–4815, 2021.
- [32] Zehao Yu, Songyou Peng, Michael Niemeyer, Torsten Sattler, and Andreas Geiger. MonoSDF: Exploring monocular geometric cues for neural implicit surface reconstruction. *NeurIPS*, 35:25018–25032, 2022.
- [33] Chong Zeng, Guojun Chen, Yue Dong, Pieter Peers, Hongzhi Wu, and Xin Tong. Relighting neural radiance fields with shadow and highlight hints. In *ACM SIGGRAPH*, pages 1–11, 2023.
- [34] Kai Zhang, Fujun Luan, Zhengqi Li, and Noah Snavely. IRON: Inverse rendering by optimizing neural sdf and materials from photometric images. In *CVPR*, pages 5565–5574, 2022.
- [35] Kai Zhang, Fujun Luan, Qianqian Wang, Kavita Bala, and Noah Snavely. PhysSG: Inverse rendering with spherical Gaussians for physics-based material editing and relighting. In *CVPR*, pages 5453–5462, June 2021.
- [36] Kai Zhang, Gernot Riegler, Noah Snavely, and Vladlen Koltun. NeRF++: Analyzing and improving neural radiance fields. *arXiv preprint arXiv:2010.07492*, 2020.
- [37] Richard Zhang, Phillip Isola, Alexei A Efros, Eli Shechtman, and Oliver Wang. The unreasonable effectiveness of deep features as a perceptual metric. In *CVPR*, pages 586–595, 2018.
- [38] Xiuming Zhang, Pratul P Srinivasan, Boyang Deng, Paul Debevec, William T Freeman, and Jonathan T Barron. NeRFactor: Neural factorization of shape and reflectance under an unknown illumination. *TOG*, 40(6):1–18, 2021.
- [39] Ruichen Zheng, Peng Li, Haoqian Wang, and Tao Yu. Learning visibility field for detailed 3D human reconstruction and relighting. In *CVPR*, pages 216–226, June 2023.
- [40] Zuo-Liang Zhu, Beibei Wang, and Jian Yang. Gs-ror: 3d gaussian splatting for reflective object relighting via sdf priors. *arXiv preprint arXiv:2406.18544*, 2024.

## A Notations

The symbols and notations are illustrated in Table 5.

Table 5: Notations in the manuscript. <sup>†</sup>Per-point variables unless being marked as *global*.

Location	Notations	Meaning
Phong model <sup>†</sup>	$I$	learnable light intensity ( <i>global</i> )
	$T_i^{light}$	received light intensity
	$k_d, k_s$	diffuse/specular coefficient
	$I_d, I_s$	diffuse/specular intensity
	$r$	point-to-light distance
	$\mathbf{n}$	normalized normal vector
Meta-learning	$\mathbf{v}$	point-to-camera normalized vector
	$\mathbf{l}$	point-to-light normalized vector
	$\theta$	Gaussian attributes
	$\theta'_i$	i-th task-specific predictor

## B Datasets

We test on three synthetic scenes and seven real-world scenes from NRHints [33], as shown in Figure 7. Each image is rendered (or captured) with a unique camera pose and point-light position. For each synthetic scene, we generate a total of 600 OLAT images using Blender, with 500 for training and 100 for testing, following either out-of-distribution or colocated data patterns to align with their settings. Specifically, the camera and light source are independently sampled on the upper hemisphere with centered around the scene, with elevation angles ranging from  $10^\circ$  to  $80^\circ$ , and radial distances uniformly sampled between  $4.0\times$  and  $5.0\times$  the object bounding size. This setup ensures a wide diversity of incident angles while maintaining plausible visibility. In the OOD configuration, training and testing light directions are drawn from non-overlapping hemispheres (azimuth  $\phi \in [0, \pi]$  for training;  $\phi \in [\pi, 2\pi]$  for testing) to induce generalization difficulty. In the colocated setting, camera and light positions are identical, emulating a mobile-light capture scenario. All images are rendered at a resolution of  $512 \times 512$  using Cycles path tracing in Blender, with 256 samples per pixel. For real captured scenes in the out-of-distribution experiment, we manually divide the data into training and testing sets, each with lights positioned on opposite sides of the upper hemisphere.

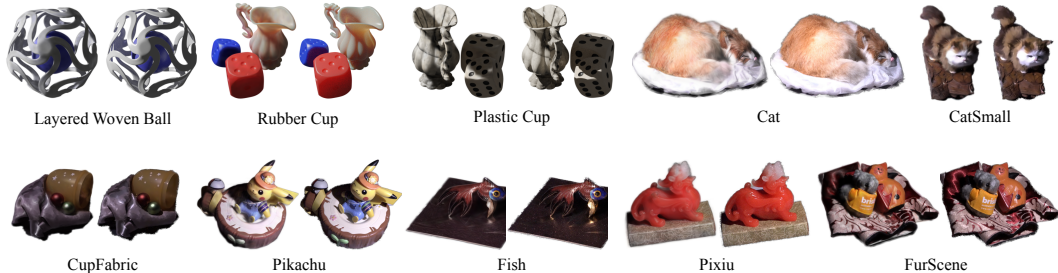


Figure 7: Synthetic and real-world scenes used in the experiment with ground-truth images (right) and rendering results of MetaGS (left).

## C More Experimental Analyses

### C.1 Full Comparisons for OOD Relighting

We present the OOD relighting results with all three metrics in Table 6 and Table 7.

### C.2 Clarification on Meta-learning

In our OLAT method, meta-learning helps mitigate overfitting to specific illuminations by explicitly simulating test conditions during training. Consider a renderer  $R(\theta, l_i)$ , where  $\theta$  represents light-

Table 6: Full comparison of the OOD relighting comparison on NRHints synthetic datasets.

Method	Layered Woven Ball			Plastic Cup			Rubber Cup		
	PSNR	SSIM	LPIPS	PSNR	SSIM	LPIPS	PSNR	SSIM	LPIPS
NRHints [33]	17.25	0.8755	0.0872	23.92	0.9485	0.0470	27.44	0.9465	0.0691
WildLight [5]	21.73	0.9217	0.0568	20.95	0.9249	0.0629	24.02	0.9221	0.0789
GS <sup>3</sup> [1]	18.84	0.9063	0.0589	20.30	0.9141	0.0628	24.37	0.9349	0.0715
Ours	<b>26.76</b>	<b>0.9561</b>	<b>0.0423</b>	<b>27.54</b>	<b>0.9580</b>	<b>0.0405</b>	<b>27.95</b>	<b>0.9497</b>	<b>0.0688</b>

Table 7: Full comparison of OOD relighting results on NRHints real-world datasets.

Method	Cat			Catsmall			CupFabric			Fish		
	PSNR	SSIM	LPIPS									
NRHints [33]	18.04	0.7821	0.2405	24.63	0.9289	0.1094	24.65	0.9377	0.0965	22.57	0.8658	0.1396
WildLight [5]	18.65	0.7293	0.2685	22.53	0.8820	0.1448	24.03	0.9246	0.0969	21.47	0.8419	0.1458
GS <sup>3</sup> [1]	17.66	0.6919	0.2431	23.34	0.9182	0.1097	25.04	0.9408	0.0954	21.12	0.8264	0.1401
Ours	<b>26.45</b>	<b>0.8514</b>	<b>0.1759</b>	<b>26.44</b>	<b>0.9505</b>	<b>0.0980</b>	<b>27.29</b>	<b>0.9490</b>	<b>0.0918</b>	<b>24.68</b>	<b>0.8706</b>	<b>0.1386</b>

Method	FurScene			Pikachu			Pixiu			Average		
	PSNR	SSIM	LPIPS									
NRHints [33]	21.55	0.8568	0.1435	24.00	0.9279	0.0958	23.03	0.8970	0.1203	22.64	0.8853	0.1351
WildLight [5]	20.33	0.8304	0.1635	19.09	0.8941	0.1129	20.22	0.8330	0.1621	20.90	0.8479	0.1564
GS <sup>3</sup> [1]	17.34	0.7684	0.1669	24.11	0.9203	0.0927	19.63	0.8391	0.1329	21.18	0.8436	0.1387
Ours	<b>24.82</b>	<b>0.8850</b>	<b>0.1297</b>	<b>25.54</b>	<b>0.9350</b>	<b>0.0928</b>	<b>25.65</b>	<b>0.9194</b>	<b>0.1105</b>	<b>25.83</b>	<b>0.9087</b>	<b>0.1196</b>

independent parameters (material/geometry), and  $l_i$  denotes the light position. Through bilevel gradients, meta-learning assesses how well the learned  $\theta'$  under  $L = \|R(\theta, l_i) - I_i\|^2$  adapts to minimizing  $\|R(\theta', l_j) - I_j\|^2$  with the simulated test condition  $l_j$ , thereby enforcing cross-illumination consistency in geometry reconstruction. This new loss function encourages the model to learn to generalize to unseen illumination rather than to overfit to a specific training sample as direct RGB loss does. By forcing geometry parameters  $\theta$  to remain consistent across  $\{l_i\}$ , we prevent illumination artifacts from being baked into textures, thereby achieving more accurate highlights and smoother surfaces. As shown in Table 8, increasing batch size (by task number) improves PSNR by 2+, while meta-learning achieves an 8+ improvement, confirming that the impact of meta-learning is not due to a larger batch size.

Table 8: A comparison of meta-learning vs. Increased batch size.

	Meta-learn	w/o Meta-Learn	Larger batch ( $\times m$ )
PSNR	27.42	19.14	20.94

### C.3 Multi-light Relighting

To validate MetaGS’s capability in handling complex lighting conditions, we conduct experiments with test sets containing 2–3 light sources. As shown in Figure 8, our method demonstrates robust generalization beyond single-light scenarios.

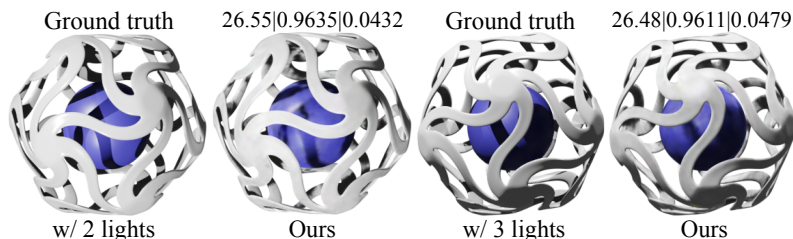


Figure 8: Results with multiple lights (PSNR/SSIM/LPIPS).

### C.4 Camera-Light-Colocated Relighting

We present the colocated relighting results with all three metrics in Table 9 and the qualitative results in Figure 9. As shown in the figure, IRON fails to accurately infer the geometry of the Layered Woven Ball scene, resulting in blurry results. In the Plastic Cup and the Rubber Cup scenes, while IRON can

Table 9: Novel view synthesis results in the **camera-light-colocated** relighting setup.

Method	Layered Woven Ball			Plastic Cup			Rubber Cup		
	PSNR	SSIM	LPIPS	PSNR	SSIM	LPIPS	PSNR	SSIM	LPIPS
IRON [34]	26.99	0.9231	0.0896	34.43	0.9808	0.0296	36.22	0.9677	0.0476
Ours	<b>38.72</b>	<b>0.9904</b>	<b>0.0124</b>	<b>36.90</b>	<b>0.9893</b>	<b>0.0145</b>	<b>38.89</b>	<b>0.9712</b>	<b>0.0385</b>

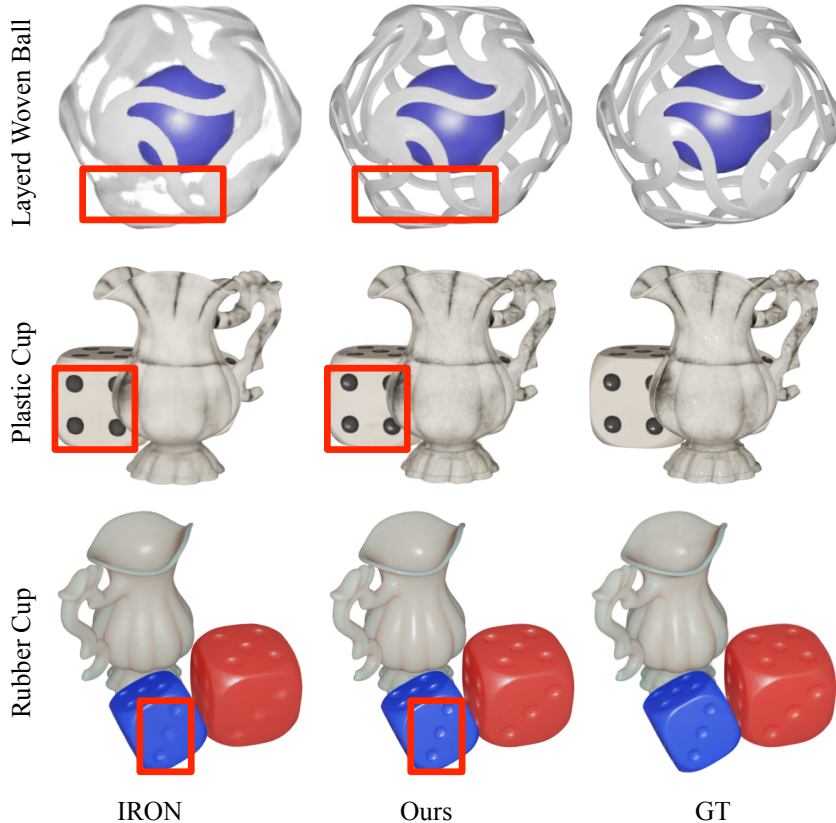


Figure 9: Novel view synthesis results under the camera-light-colocated relighting setup. Compared to IRON, our model more accurately infers object geometry in the Layered Woven Ball scene and produces fewer artifacts in the Plastic Cup scene.

provide reasonable geometry reconstruction, it shows more artifacts in the appearance modeling, such as the dent of the dice. On the other hand, MetaGS can provide more accurate illumination details.

### C.5 In-distribution Novel View Relighting

This experiment follows the setup in NRHints [33], where both training and testing lights are randomly located in the upper hemisphere surrounding the scene). Each view is illuminated by a single point light placed at a unique position, though all light positions are distributed within the same region. During the testing phase, we evaluate on novel viewpoints under *new, in-distribution* light positions. Similar to the OOD setting, we generate 600 OLAT images per synthetic scene using Blender (500 for training and 100 for testing). For real-world scenes, we use only 600 training images—a significantly smaller subset compared to the full NRHints dataset.

We present the quantitative results for free-viewpoint relighting with in-distribution point light positions in Table 10. Notably, MetaGS outperforms other near real-time methods, including Relightable 3DGS and GaussianShader, by large margins, and shows an advantage over GS<sup>3</sup>, a Gaussian-based OLAT method. Our method underperforms NRHints on certain “not-so-difficult” datasets such as *PlasticCup* and *RubberCup*. This is partly because the implicit rendering model in NRHints provides better color fitting, resulting in superior in-distribution performance. While

Table 10: Novel view synthesis results in the in-distribution relighting setup. We present the best and second-best results in bold and underlined format, respectively.

Method	Layered Woven Ball			Plastic Cup			Rubber Cup			Average		
	PSNR <sup>↑</sup>	SSIM <sup>↑</sup>	LPIPS <sup>↓</sup>	PSNR <sup>↑</sup>	SSIM <sup>↑</sup>	LPIPS <sup>↓</sup>	PSNR <sup>↑</sup>	SSIM <sup>↑</sup>	LPIPS <sup>↓</sup>	PSNR <sup>↑</sup>	SSIM <sup>↑</sup>	LPIPS <sup>↓</sup>
3DGS [9]	19.55	0.9130	0.0580	21.13	0.9417	0.0470	23.22	0.9248	0.0796	21.30	0.9265	0.0615
Relightable 3DGS [7]	19.62	0.9088	0.0610	21.07	0.9390	0.0502	23.20	0.9224	0.0838	21.30	0.9234	0.0650
GaussianShader [8]	19.62	0.9137	0.0586	20.92	0.9394	0.0500	23.12	0.9241	0.0833	21.22	0.9257	0.0640
NRHints [33]	18.99	0.9087	0.0731	<b>35.81</b>	<b>0.9847</b>	<b>0.0281</b>	<b>36.64</b>	<b>0.9637</b>	<b>0.0481</b>	<u>30.48</u>	<u>0.9524</u>	<u>0.0498</u>
WildLight [5]	22.71	0.9284	0.0499	23.28	0.9068	0.1018	24.65	0.9271	0.0737	23.55	0.9208	0.0751
GS <sup>3</sup> [1]	<u>28.20</u>	<u>0.9659</u>	<u>0.0396</u>	29.53	0.9755	0.0317	29.34	0.9520	0.0618	29.02	0.9645	0.0444
Ours	<b>30.88</b>	<b>0.9690</b>	<b>0.0281</b>	<u>32.51</u>	<u>0.9814</u>	<u>0.0295</u>	<u>31.75</u>	<u>0.9577</u>	<u>0.0570</u>	<b>31.71</b>	<b>0.9694</b>	<b>0.0382</b>

the Phong-based rendering model used in our work facilitates geometry-shading decoupling and is particularly effective for objects with incoherent geometries, such as the *Woven Ball*. However, does NRHints truly learn the intrinsic reflection mechanisms from the observed images? Likely not, as evidenced in the previous OOD results.

## D Preliminaries

### D.1 3D Gaussian Splatting

Our method builds upon 3D Gaussian Splatting (3DGS) [9], which employs explicit Gaussian points for 3D scene representation. Each Gaussian’s geometry is characterized by an opacity  $o \in [0, 1]$ , a center point  $\mu \in \mathbb{R}^{3 \times 1}$  and a covariance matrix  $\Sigma \in \mathbb{R}^{3 \times 3}$ :

$$G(\mathbf{X}) = e^{-\frac{1}{2}(\mathbf{X}-\mu)^T \Sigma^{-1}(\mathbf{X}-\mu)}, \quad (4)$$

where the covariance matrix  $\Sigma$  can be decomposed into a scaling matrix  $S \in \mathbb{R}^{3 \times 1}$  and a quaternion-parameterized rotation matrix  $R \in \mathbb{R}^{3 \times 3}$  for differentiable optimization:

$$\Sigma = RSS^T R^T. \quad (5)$$

To render an image from a given viewpoint, 3DGS uses the splatting technique to cast Gaussians within the view frustum onto the camera plane. The projected 2D covariance matrix  $\Sigma'$  in camera coordinates can be computed as  $\Sigma' = JW\Sigma W^T J^T$ , where  $W$  and  $J$  denote the viewing transformation and the Jacobian of the affine approximation of the projective transformation, respectively. The color of each pixel  $\mathbf{p}$  is calculated by alpha-blending  $N$  ordered Gaussians  $\{G_i | i = 1, \dots, N\}$  overlapping  $\mathbf{p}$  as:

$$\mathcal{C} = \sum_{i \in N} T_i \alpha_i \mathbf{c}_i \text{ with } T_i = \prod_{j=1}^{i-1} (1 - \alpha_j), \quad (6)$$

where  $\alpha_i$  denotes the alpha value calculated by multiplying the opacity  $o$  with the 2D Gaussian contribution value derived from  $\Sigma'$ , and  $T_i$  denotes the accumulated transmittance along the ray.

Specifically, each Gaussian’s color is defined by spherical harmonics (SH) coefficients  $\mathcal{C} \in \mathbb{R}^k$  (where  $k$  represents the degrees of freedom). While high-order SH coefficients can contribute to the overall lighting of a scene under various view directions, they are not specifically designed to handle view-dependent color directly, such as specular reflections and shadows.

### D.2 Blinn-Phong Reflection Model

The Phong model is widely adopted in computer graphics for simulating the interaction of light with object surfaces [18]. In this model, the reflected light transport on a surface has three components: ambient ( $L_a$ ), diffuse ( $L_d$ ), and specular reflections ( $L_s$ ). The ambient reflection component represents the constant illumination present in the environment, simulating how light scatters and reflects off other surfaces to establish a baseline brightness level. The diffuse reflection component, governed by Lambertian diffusion law, illustrates the scattering of light in multiple directions upon striking a rough surface, leading to a matte appearance. This component is calculated based on the angle between the light direction ( $\mathbf{l}$ ) and the surface normal ( $\mathbf{n}$ ), ensuring that surfaces facing the light source appear brighter. The specular term is computed based on the angle between the light

Table 11: Hyperparameters of MetaGS.

Name	Notation	Value
learning rate	$\beta$	same as 3DGS [9]
meta-train inner learning rate	$\alpha$	0.01
meta-train task number	$m$	5
RGB D-SSIM loss scale	$\lambda$	0.2
sparse loss scale	$\lambda_{\text{sparse}}$	0.001
normal prediction loss scale	$\lambda_n$	0.2
normal residual loss scale	$\lambda_{\text{res}}$	0.001
flatten loss scale	$\lambda_s$	0.001

direction vector and the bisector ( $\mathbf{h}$ ) between the view direction ( $\mathbf{v}$ ) and the light direction ( $\mathbf{l}$ ). The Phong model also incorporates a shininess exponent that governs the spread of the specular highlight, allowing the model to represent the surface’s glossiness. We select the Blinn-Phong model [2] to provide the illumination decomposition priors to 3DGS for its simple yet strong physical prior and computation efficiency. With little addition to the Gaussian’s attribute, our model produces realistic lighting effects.

## E Hyperparameters

Table 11 presents the hyperparameters of MetaGS.